RSC Advances

ROYAL SOCIETY OF CHEMISTRY

www.rsc.org/advances

Graphical abstract

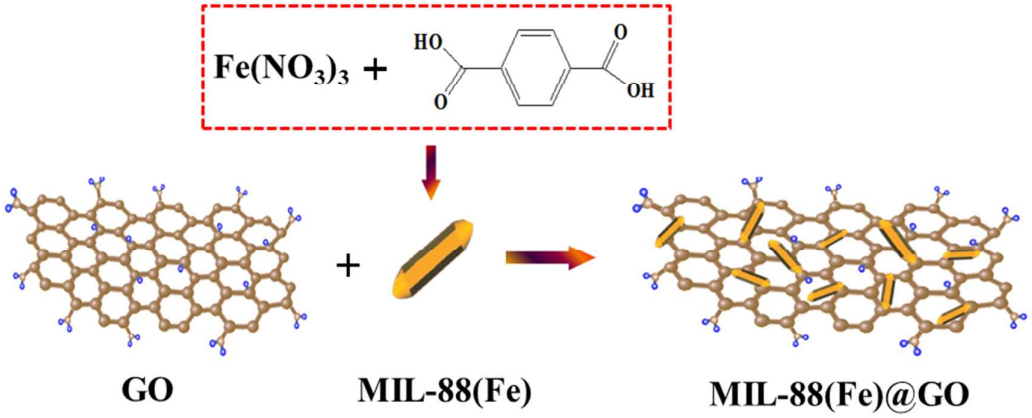

Iron(III)-based metal−organic framework/graphene oxide composites were prepared and afforded fast degradation performance and high catalytic efficiency for dyes.

RSC Advances

RSCPublishing

COMMUNICATION

Synthesis of iron (III)-based metal−organic framework /graphene oxide composites with increased photo-catalytic performance for dye degradation

Cite this: DOI: 10.1039/x0xx00000x

Received ooth January 2012,
Accepted ooth January 2012

DOI: 10.1039/x0xx00000x

www.rsc.org/

Yan Wu[ab], Hanjin Luo[*ab], Hou Wang[c]

To improve the utilization efficiency of MOF catalyst, Iron(III)-based metal−organic framework/graphene oxide composites were prepared by a facile method. The composites afforded fast degradation performance and high catalytic efficiency for degradation of methylene blue and rhodamine B under exposure to natural sunlight.

Metal-organic frameworks (MOFs), formed by coordination bonds between metal clusters and organic linkers, have shown significant potential for hydrogen storage, gas sorption and separation, and catalysis due to their high specific surface areas and tunable pore sizes.[1] More efforts have been made to fabricate MOFs based hybrid composites for analytical applications, such as n-alkanes separation,[2] polycyclic aromatic hydro-carbons extraction,[3] electrocatalytic oxidation,[4] and lead ion sensing.[5] MOFs can consist of Fe(III)-oxide clusters, linked together in three dimensions by organic linkers. Several MOFs are known that contain Fe_3-μ_3-oxo clusters as a structural motif, with a great variety in topology and pore sizes depending on the organic linker and preparation conditions used. Graphene is the most recent member of the multi-dimensional carbon-nanomaterial family. As one of the most important derivatives of graphene, graphene oxide (GO) has attracted significant attention in multidisciplinary field owing to the advantages of large surface area, excellent conductivity and strong mechanical strength.[6] However, the combination of metal-organic frameworks with graphene oxide (MOF@GO) as a selective catalyst has not been explored until now. The purpose of this study is to examine the feasibility of MOF@GO hybrid composites for the application in degradation of methylene blue and rhodamine B.

In this article, we demonstrated a facile and rapid single step method for synthesis of iron(III)-based MOFs(MIL-88(Fe)) with graphene oxide. The resulting hybrid composites (MIL-88(Fe)@GO) was characterized by Fourier transform infrared spectroscopy (FTIR), Raman spectroscopy, powder X-ray diffraction (XRD), scanning electron microscopy (SEM), X-ray photoelectron spectroscopy (XPS), diffuse-reflectance UV−vis spectroscopy and thermogravimetric analysis (TGA). The catalytic activity of MIL-88(Fe)@GO catalyst has been explored through degradation of two important dyes, methylene blue (MB) and rhodamine B (RB) under exposure to natural sunlight. The average intensity of sunlight was measured using Light Meter (LX1010B), which was found to be 760–840 W/m^2. The photocatalytic experiment was performed in natural atmosphere, without any external source of aeration.

GO was synthesized from natural graphite by a modified Hummers method according to our previous reports.[7] MIL-88(Fe) was prepared by mixing 1,4-benzenedicarboxylic acid (BDC) and $Fe(NO_3)_3{\cdot}9H_2O$. The overall procedure of preparation of MIL-88(Fe)@GO catalysts has been schematically depicted in Scheme 1.

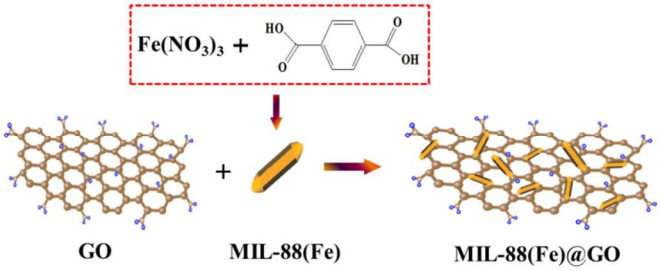

Scheme 1. Illustration for the preparation of MIL-88(Fe)@GO

The morphological details were identified by SEM images (Fig. 1). The morphology of MIL-88(Fe) (Fig. 1(a)) had the appearance of rod, with particle size smaller than 2 μm in length, which is not very well-distributed. After reacting with GO, MIL-88(Fe)@GO (Fig. 1(b)) moderately maintains the

original rod-shape of the MIL-88(Fe), indicating that the addition of GO in the preparation of the MIL-88(Fe)@GO had no effect on the morphology of the MIL-88(Fe). Furthermore, some obvious wrinkles or layered-structures in accordance with the characteristic of GO were observed, suggesting that the MIL-88(Fe) had been "wrapped" by GO.

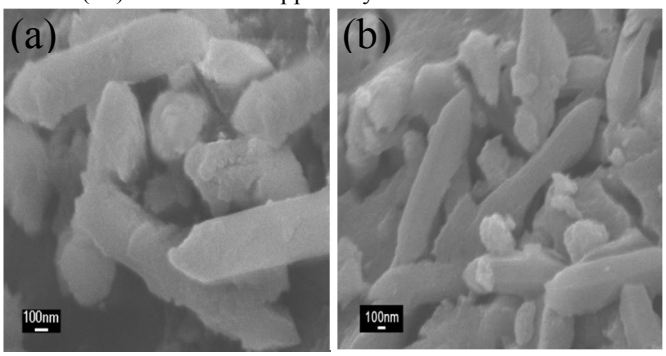

Fig. 1. The SEM images of MIL-88(Fe) (a) and MIL-88(Fe)@GO (b)

In XRD patterns of the MIL-88(Fe)@GO sample (Fig. 2(a)), the sharp peak at 12° can be assigned to the plane of the multilayer GO sheets, [8] which thus proved the existence of the graphene oxide in the MIL-88(Fe)@GO. Compared with the XRD patterns of MIL-88(Fe), MIL-88(Fe)@GO resulted in a small change in the peak position and intensity. This phenomenon is attributed to the exfoliation/dispersion of GO in the polar solvents used during the material preparation.[9]

The Raman spectrum was recorded to demonstrate the change that occurred in the structure of the MIL-88(Fe)@GO as compared with GO (Fig. 2(b)). The intensity ratio of D and G bands is a measure of the relative concentration of sp^3 hybridized defects compared to the sp^2 hybridized graphene domains, and the lower value of I_D/I_G indicates the lower defects and disorders of the graphitized structure.[10] The I_D/I_G ratio of MIL-88(Fe)@GO (1.34) is obviously higher than that of GO (1.02), which indicates that more graphitization and more sp^2 bonds form after interaction with MIL-88(Fe). The two obvious peaks for GO at 1331.38 and 1585.88 cm^{-1} correspond to the D and G band, respectively. Moreover, it can be seen that the peak of D and G band was red-shifted to 1342.77 and 1599.24 cm^{-1} for MIL-88(Fe)@GO. The red-shift of D and G band was mainly caused by the electronic inter-action between MIL-88(Fe) and GO with a firm interface.[11]

The functional groups present in the MIL-88(Fe) and MIL-88(Fe)@GO are characterized by FTIR and shown in Fig. 2(c). As for MIL-88(Fe), the peaks at 1496 and 1386 cm^{-1} are attributed to the symmetric stretching of carboxylate group in the BDC linker.[12] The peak appeared at 1496 cm^{-1} is produced by a combination of benzene ring stretching and deformation modes, and the peak around 675 cm^{-1} is related to bending vibration of C-H. The peak at 1608 cm^{-1} is related to a resonance peak of C–C stretching and absorbed hydroxyl groups. The FTIR absorption band observed at 1022 cm^{-1} is assigned to a Fe–N stretching vibrational mode. After GO incorporation, the high intensity MIL-88(Fe) peak swamped the characteristic GO peak due to the rather small content of GO. Hence, the FTIR spectrum of MIL-88(Fe)/GO are similar to that of MIL-88(Fe), excepted that two additional bands which emerge at 2782 and 3022cm^{-1}, which can be assigned to saturated and unsaturated C-H stretching vibration respectively.

The thermal stability of the sample was tested by TGA. The weight loss occurred below 150℃ for GO (Fig. 2(d)) was attributed to desorption of physisorbed water and the major weight loss observed for GO around 180℃ was ascribed to removal of oxygen-containing groups accompanied by the liberation of CO_x and H_2O species.[13] As shown in Fig. 2(d), MIL-88(Fe) and MIL-88(Fe)@GO exhibit similar thermal behavior. There was a rapid weight drop before 220℃ in both MIL-88(Fe) and MIL-88(Fe)@GO that attributed to the loss of the residual (or absorbed) solvent and the decomposition of residual organic functional groups on MIL-88(Fe) and MIL-88(Fe)@GO,[14] and then weight drop to 13.4% and 10.1% before 360 ℃ for MIL-88(Fe) and MIL-88(Fe)@GO, respectively, which means the collapsion of the framework.[15] At this temperature, the material lost its crystal structure, and become amorphous. The differences observed in the thermal behavior of GO, MIL-88(Fe) and MIL-88(Fe)@GO indicate that their structures are different.

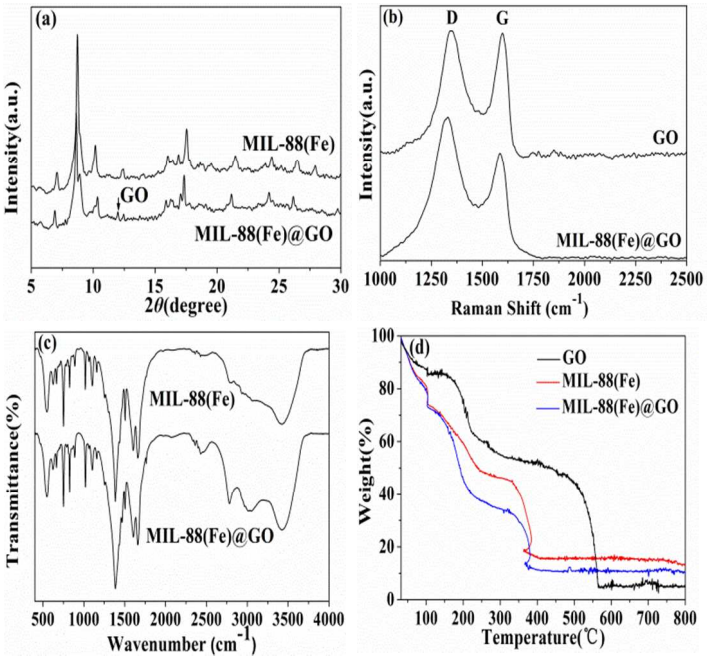

Fig. 2.(a) The XRD patterns of MIL-88(Fe) and MIL-88(Fe)@GO; (b) The Raman spectra of MIL-88(Fe) and MIL-88(Fe)@GO; (c) The FTIR spectra of MIL-88(Fe) and MIL-88(Fe)F@GO; (d) The TGA curves of GO, MIL-88(Fe) and MIL-88(Fe)@GO

Fig. 3 shows the XPS spectra of survey, C 1s, and Fe 2p for MIL-88(Fe) and MIL-88(Fe)@GO. The full survey (Fig. 3a) of the surface composition for MIL-88(Fe) and MIL-88(Fe)@GO shows photo electron lines at a binding energy of about 284.6, 531.6, and 711.1 eV, which may be attributed to C 1s, O 1s, and Fe 2p, respectively. Deconvolution of the C 1s peak (Fig.

3b and 3c) of MIL-88(Fe) and MIL-88(Fe)@GO shows three peaks at about 284.9, 286.1, and 288.0 and 289.5 eV, corresponding to C–C, C–O, C=O and O–C=O groups,[16] respectively. From the (Fig. 3b and 3c), we can know the C–C in MIL-88(Fe)@GO increases significantly than MIL-88(Fe) but the C–O, C=O and O–C=O groups are much less than MIL-88(Fe), which implies that GO has been successfully conjugated on MIL-88(Fe). The spectrum of Fe 2p for MIL-88(Fe) (Fig. 3d) shows three peaks at 710.6, 715.7 and 723.5 eV, which are all corresponding to α-Fe_2O_3.[17] Furthermore, the spectrum of Fe 2p for MIL-88(Fe)@GO (Fig. 5d) also shows three peaks at 710.6, 713.1 and 723.6 eV, and the peak at 713.1 eV corresponding to the characteristic peak of $Fe_2(SO_4)_3$. The existence of sulfate would be a consequence of sulfuric acid treatment in the GO preparation process, suggesting that GO has been successfully conjugated on MIL-88(Fe) further.[18]

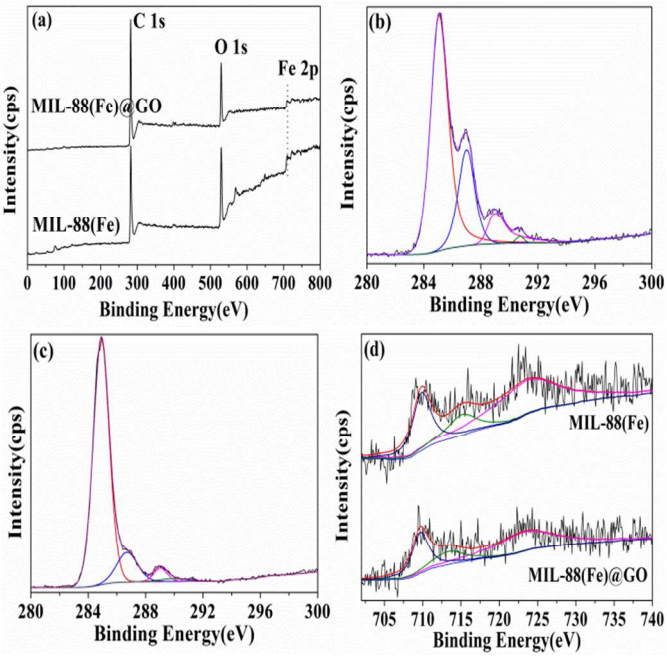

Fig. 3. The XPS spectra of (a) full survey of MIL-88(Fe) and MIL-88(Fe)@GO; (b) C 1s core levels of MIL-88(Fe); (c) C 1s core levels of MIL-88(Fe)@GO; (d) Fe 2p core levels of MIL-88(Fe) and MIL-88(Fe)@GO

The catalytic activity of GO, MIL-88(Fe) and MIL-88(Fe)@GO catalyst was evaluated by degradation of MB and RB under exposure to natural sunlight. Fig. 4(a) and (b) show the degradation performance of MB and RB in presence of GO, MIL-88(Fe) and MIL-88(Fe)@GO catalyst at different time of exposure to sunlight. In the absence of catalyst, the degradation of MB and RB was negligible even after long-time irradiation, which indicates that the self-photosensitization of MB and RB could be absolutely low. From Fig. 4(a), the MB was completely degraded by MIL-88(Fe)@GO, GO and MIL-88(Fe) catalysts at 20, 40 and 50 min of exposure, respectively. From Fig. 4(b), the RB was completely degraded by MIL-88(Fe)@GO, GO and MIL-88(Fe) catalysts at 30, 40 and 60 min of exposure, respectively. Under identical experimental conditions, the catalytic efficiency of MIL-88(Fe)@GO catalyst for both MB and RB was found to be higher than GO and MIL-88(Fe) catalyst. The existence of GO in MIL-88(Fe)@GO catalyst not only catalyze the degradation of MB and RB but can also adsorb the MB and RB molecules.[19]

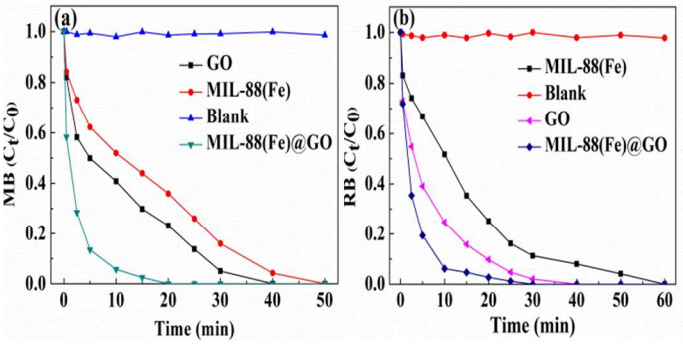

Fig.4. Effect of contact time on the degradation rate of MB (a) and RB (b) by GO, MIL-88(Fe) and MIL-88(Fe)@GO

In conclusion, we have successfully fabricated the MIL-88(Fe)@GO composites by a facile, efficacious and environment-friendly method. The MIL-88(Fe)@GO composites demonstrate the fast MB and RB degradation performance with an almost complete degradation of MB and RB within 20 and 30 min, respectively. Furthermore, the as-prepared MIL-88(Fe)@GO composites could improve the catalytic efficiency greatly for the degradation of MB and RB than MIL-88(Fe) and GO. This study showed the as-prepared MIL-88(Fe)@GO composites could be utilized as the efficient adsorbent for the environmental cleanup.

This work was financially supported by National Natural Science Foundation of China (No. 40973074).

Notes and references

[a]*College of Environment and Energy, South China University of Technology, Guangzhou 510006, P.R. China. E-mail: wuyan1101@126.com.*
[b]*The Key Laboratory of Pollution Control and Ecosystem Restoration in Industry Clusters of Ministry of Education, Guangzhou 510006, P.R. China. E-mail: luohj@scut.edu.cn.*
[c]*College of Environmental Science and Engineering, Hunan University, Changsha 410082, PR China. E-mail: huankewanghou024@163.com.*
†Electronic supplementary information (ESI) available: Materials, synthetic procedures and characterization. See DOI: 10.1039/ b000000x/

1 (a) L. Bromberg, X. Su, T. A. Hatton, *ACS Appl. Mater. Interfaces*, 2013, **5**, 5468; (b) D. F. Liu, Y. S. Lin, Z. Li, H. X. Xi, *Chem. Eng. Sci.*, 2013, **98**, 246; (c) P. Pachfule, R. Banerjee, *Cryst. Growth Des.*, 2011, **11,** 5176.
2 N. Chang, Z. Y. Gu, H. F. Wang, X. P. Yan, *Anal. Chem*, 2011, **83**, 7094.
3 (a) S. H. Huo, X. P. Yan, *Analyst*, 2012, **137**, 3445; (b) X. F. Chen, H. Zang, X. Wang, J. G. Cheng, R. S. Zhao, C. G. Cheng, X. Q. Lu, *Analyst,* 2012, **137,** 5411.
4 H. Hosseini, H. Ahmar, A. Dehghani, A. Bagheri, A. R. Fakhari, M. M. Amini, *Electrochim. Acta*, 2013, **88**, 301.
5 Y. Wang, Y. C. Wu, J. Xie, H. L. Ge, X. Y. Hu, *Analyst*, 2013, **138**, 5113.
6 H. Wang, X. Yuan, Y. Wu, H. Huang, X. Peng, G. Zeng, H. Zhong, J. Liang, M. Ren, *Adv. Colloid. Interface Sci.*, 2013, **195–196,** 19.

7 Y. Wu, H. J. Luo, H. Wang, C. Wang, J. Zhang, Z. L. Zhang, *J. Colloid Interface Sci.*, 2013, **394**, 183.
8 H. Wang, X. Z. Yuan, Y. Wu, H. J. Huang, G. M. Zeng, Y. Liu, X. L. Wang, N. B. Lin, Y. Qi. *Appl. Surf. Sci.*, 2013, **279**, 432.
9 T. J. Bandosz, C. Petit, *Adsorption,* 2011, **17**, 5.
10 (a) O. Akhavan, M. Abdolahad, A. Esfandiar and M. Mohatashamifar, *J. Phys. Chem. C*, 2010, **114,** 12955; (b) O. Akhavan, *ACS Nano*, 2010, **4**, 4174; (c) Y. Zhang, Z. Tang, X. Fu and Y. Xu, *ACS Nano*, 2011, **5**, 7426.
11. E. P. Gao, W. Z. Wang, M. Shang, J. H. Xu, *Phys. Chem. Chem. Phys*. 2011, **13,** 2887.
12 Y. Wang, Y, C. Wu, H. L. Ge, H. H. Chen, G. Q. Ye, X. Y. Hu, *Talanta,* 2014, **122** 91.
13 G. Jiang, Z. Lin, C. Chen, L. Zhu, Q. Chang, N. Wang, W. Wei, H. Tang, *Carbon*, 2011, **49,** 2693.
14 S. Stankovich, D. Dikin, R.D. Piner, K.A. Kohlhaas, A. Kleinhammes, Y. Jia, Y. Wu, S.T. Nguyen, R.S. Ruoff, *Carbon,* 2007, **45** 1558.
15 M. Anbia, V. Hoseini, *Chem. Eng. J.* 2012,**191,** 326.
16 C. Wang, H. J. Luo, Z. L. Zhang, Y. Wu, J. Zhang, S. W. Chen. *J. Hazard. Mater.,* 2014, **268**, 124.
17 J. Lu, X. L. Jiao, D. R. Chen, W. Li, *J. Phys. Chem. C,* 2009, **113**, 4012.
18 Z. H. Huang, G. Q. Liu, F. Y. Kang, *ACS Appl. Mater. Interfaces,* 2012, **4,** 4942.
19 B. Li, H. Cao, *J. Mater. Chem.*, 2011, **21,** 3346.

